We are IntechOpen,
the world's leading publisher of
Open Access books
Built by scientists, for scientists

6,900
Open access books available

185,000
International authors and editors

200M
Downloads

154
Countries delivered to

Our authors are among the

TOP 1%
most cited scientists

12.2%
Contributors from top 500 universities

BOOK CITATION INDEX
CLARIVATE ANALYTICS
INDEXED

WEB OF SCIENCE™

Selection of our books indexed in the Book Citation Index
in Web of Science™ Core Collection (BKCI)

Interested in publishing with us?
Contact book.department@intechopen.com

Silver Particulate Films on Compatible Softened Polymer Composites

Pratima Parashar

Additional information is available at the end of the chapter

1. Introduction

Polymer/inorganic nanocomposites have been of great interest in recent years, not only for the novel properties of the nanocomposite materials but also for the continuously growing demand for the miniaturisation of electronics components, optical detectors, chemicals and biochemical sensors and devices.

Polymer matrices have been frequently used as particle stabilizers in chemical synthesis of metal colloids since these prevent agglomeration of the particles. Within the past decade, incorporating silver nanoparticle into a polymer matrix is more interesting because the resulting nanocomposites exhibit applications in catalysis, drug wound dressing and optical information storage.

It is difficult to disperse silver nanoparticle homogeneously into a polymer matrix by ex situ methods because of easy agglomeration of nanoparticles. At present, it is possible to obtain nanoparticles of different shape and size in nanostructured polymeric environment using various polymeric systems and different approaches. Numerous methods used toxic and potentially hazardous reactants. Increasing environmental concerns over synthesis route resulted in an attempt to adopt eco friendly methods.

One of the simplest techniques to form such particulate structures, which are generally known as island or discontinuous metal films, is through vacuum evaporation of metal on to a dielectric substrate by stopping the deposition at a very early stage. The temporal instability exhibited by island films even in vacuum is attributed to mobility of islands followed by coalescence [1]. Further, these films get oxidised when they are exposed to atmosphere. The oxidation of islands causes an irreversible increase in electrical resistance [2]. An interesting sub-surface particulate structure formation was reported when certain inorganic materials are deposited on to softened polymer substrates [3-6] and the

morphology and formation of such structures depend on thermodynamic as well as deposition parameters [6, 5]. The use of softened polymer substrats provides the unique possibility of easily controlling the viscosity of the substrate to form a subsurface discontinuous silver particulate films. The morphology of sub-surface particulate structures also depends upon polymer metal interaction [7, 8]. The reported method is evaporation of silver on polymer substrate at high temperature and in vacuum of the order of 10^{-6} Torr. The ability to precisely tailor and optimize the nanocomposite structure creates opportunities for a wide range of applications.

2. Body

Pyridine-containing polymers have attracted interests in recent years because they can be used in various applications as water-soluble polymers and coordination reagents for transition metals, especially 4-vinylpyridine because of its more interesting properties resulting from higher accessibility of the nitrogen atom [9].

Deposition of silver on interacting polymers like Poly (2-vinylpyridine) and Poly (4-vinylpyridine) resulted in the formation of smaller particles (~ a few tens of nm) with smaller inter-particle separations whereas silver deposited on softened inert polymer like polystyrene (PS), irrespective of the deposited thickness is of highly agglomerated structures. Therefore, silver films on inert polymer lack in application due to room temperature resistances equalling that of the substrate. But, silver films on interacting polymers have room temperature resistance in the range of a few tens to a few hundred $M\Omega$/sheet, which is desirable for device applications [8]. Both the interacting polymers are hygroscopic and costly. Therefore, blending an inert and stable polymer like PS with interacting polymers like P2VP and P4VP may provide a polymer matrix suitable for formation of subsurface silver films. Miscibility between the components polymers play a vital role in blending of polymers at the molecular levels. A compatible blend provides a firm basis for further application in devices. Earlier researchers [10-14] have suggested the improvement of miscibility of PS with P4VP by incorporating proton donors like poly (acrylic) acid and poly (p-vinyl phenol) or methacrylic acid into the chains of PS with P4VP in order to utilise its proton acceptor nature. Further, reversible addition-fragmentation chain transfer polymerization was developed by J.J. Yuan and et al [9] for the controlled preparation of PS/P4VP triblock copolymers as PS-b-P4VP-b-PS and P4VP-b-PS-b-P4VP.In order to retain the properties of both the polymers PS and P4VP, blending is carried out through solution casting and it is expected that combination of PS and P4VP should give rise to organised subsurface silver particulate structures with the advantages of both the polymers.

Polymer blending is a common way to develop new polymer materials with desirable combinations of properties. The main advantage of this method is to control the properties by varying the blend compositions [15]. A compatible blend is needed to have desirable combinations of properties of both the polymers. Compatibility of the two homopolymers is needed to an optimum extent for a blend to show superior properties. The compatibility signifies specific interaction such as dipole-dipole, ion-dipole and hydrogen bonding.

Various measurements like heat of mixing, viscometry, glass transition temperature, morphological studies by optical and electron microscopy, infrared spectroscopy and dynamic mechanical analysis, are used to study polymer compatibility. The compatibility of polymer composite is discussed using DSV, DSC, FTIR and SEM. Dilute solution viscometry is a simple and reliable method to investigate interactions of macromolecules in solution. It has been used as a complementary technique to prospect the effect of the position of nitrogen atom in the pyridine ring of P4VP on the interaction developed within PS/P4VP blends. This technique could not be applied to PS/P2VP blends because these blends show phase separation after twenty-four hour of preparation of solution. The criterion of single composition dependent glass transition is used to investigate the miscibility of polymer blends by DSC. Specific interactions most often liberate a heat of mixing and contribute towards the free energy of mixing. Fourier transform infrared spectroscopy is used to investigate specific interactions between the homopolymers in the blend compositions and compared to calorimetric results. SEM results confirm compatibility of blends at higher temperature.

Nanocomposites of metal nanoparticles in a polymer matrix have generated a great deal of interest which depends on the metal-polymer composition and their structure. Polymers are particularly attractive as the dielectric matrix in composites due to their versatile nature and can easily be processed into thin films. These nanocomposites exhibit a unique combination of desirable optical and electrical properties that are otherwise unattainable [16-20].All these properties depend on the size, size distribution and shape of the nanoparticles. The growth and arrangement of metal nanoparticles on various substrates are therefore key issues in all the fields of modern science and technology relating to nanoelectronics, photonics, catalysis and sensors [21].
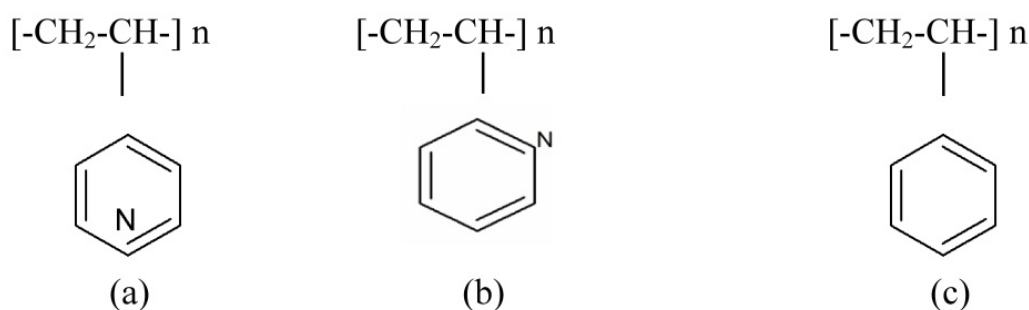
Since past, polymer membranes have been studied as supporting materials for colloidal metals which are well known catalysis. Strictly speaking, such a membrane contained colloidal metal-rich and metal-poor phases and the localization of colloidal metals is governed by non–linear diffusion equations. Poly (styrene-b-2-vinyl pyridine) diblock copolymer forms micro phase separated film [22] and Ag ion added to such a film is localized in P2VP micro domains not in PS phase. Theoretical study in the self assembly of inorganic/block copolymers hybrids by Ginzburg and co-workers have predicted that affinity, size and amount of inorganic nanoparticles can be exploited to control the phase behaviour of inorganic/BCP hybrids [23].

Metal–polymer nanocomposite containing widely separated nanoparticles exhibit insulating behaviour. As the percentage of metal in composite increases, the nanoparticle separation decreases. At a certain thickness of silver on softened polymer substrate, nanoparticles are quite densely packed but separated by polymer gap such a film offer a host of unique property relevant to practical applications. These applications include high dielectric constant passives, electromagnetic interference shielding, sensors, and detector designed for a variety of specific purposes with high performances, sensitivity and flexibility [24]. Further, the morphology of the cluster films deposited on softened polymer substrates is dependent on the polymer-metal interaction. Gold deposited on polystyrene (PS) and

subsequently annealed above its glass transition temperature results in a highly agglomerated film with large separation between the clusters, possibly due to inert nature of PS [1]. Silver deposited on PS also forms highly agglomerated subsurface particulate structure with large separations between the metal particles [25].Also, coalescence rate for gold particles in a poly(2-vinyl pyridine) matrix is much less than the coalescence rate for gold particles in a polystyrene matrix, indicating that homopolymer/metal interactions play an important role in the determination of the coalescence rate [7].Hence, this high coalescence rate in case of PS resulted in a highly agglomerated film even for a thickness of 300 nm. But, silver deposited on an interacting polymer like Poly (2-vinylpyridine) and poly (4-vinylpyridine) resulted in the formation of smaller particles (~ a few tens of nm) with smaller inter-particle separations [8].The differences in dispersion, size distribution and impregnation depth result from the differing natures of the polymer hosts and the processing conditions [26]. Therefore, it is desirable to restrict the nanoparticles to a small size regime along with a narrow size distribution by blending inert PS with interacting P2VP and P4VP.Therefore; it is interesting to blend PS with P2VP and P4VP in order to have desired morphology of silver particulate films on compatible polymer composite.

3. Experimental

Poly (4-vinyl pyridine) and Poly (2-vinylpyridine) used in this study, were procured from Sigma-Aldrich Chemicals Pvt. Ltd and Polystyrene from Alfa-Aesar (A Johnson Mathley company) respectively. The molecular weights of P4VP, P2VP and PS are 60,000, ~37,500 and 100,000, respectively. The structure of P4VP, P2VP and PS are (a), (b) and (c), respectively, as follows:

Polymer blends were prepared through solution blending by mixing in a common solvent, dimethylformamide (DMF). Blends of PS/P4VP with different compositions {PS (w)/P4VP (w) =0:100; 25:75, 50:50; 75:25; 100:0} were prepared. 1g of the total polymers at different ratios was dissolved in 20 ml of DMF at room temperature. Composite of PS/P2VP with different compositions {PS (w)/P2VP (w) = 0:100; 50:50; 100:0} were prepared. An amount of 0.5 g of the total polymers at different ratios, were dissolved in 5 ml of DMF at room temperature.

The stock solutions of PS, P4VP, and their different blend compositions were prepared in the common solvent DMF. Viscosity measurements were made using Ubbelohde Viscometer at 28^0C with an accuracy of ±0.2%.

For DSC study, the solvent is allowed to evaporate in a thermostat for 24 hours. The residuals of component polymers and their blend in powder form were then dried at 80^0 C for several days to ensure complete removal of any traces of residual solvent. The residuals of component polymers and their blends were found to be translucent. DSC measurements were carried out using a Shimadzu DSC-50. Small quantities of the samples, 8-10 mg were scanned at a heating rate of 5- 10 K/min^{-1} in the temperature range 28 to 220^0C under Nitrogen, N_2.

FTIR spectra of the blends were recorded using a Perkin-Elmer spectrometer (model 1000).

Thin films of homopolymers and their composite of approximately 5μm thickness were solution cast on a glass slide pre-coated with silver contacts with a gap of 1 cm X 1 c m for electrical studies. Silver films of various thicknesses were deposited on these substrates held at 457 K in a vacuum better than 8×10^{-6} Torr. The glass transition temperature of P4VP, P2VP and PS are 410, 357 and 373 K, respectively. Therefore, polymer substrates are softened at 457 K and sufficient fluidity is ensured. A chromel-alumel thermocouple was used to measure the substrate temperature by clamping it to the substrate surface holding the film. Source to substrate distance was maintained at 20 cm. A Telemark quartz crystal monitor (Model 850) was used to measure the deposition rate, as well as the overall film thickness. The deposition rate used was 0.4nm/s for all the films. Resistance measurements were carried out in-situ, using a Keithley electrometer model 617. The films were annealed at the deposition temperature for 1 hour before cooling them to room temperature. Stability of the films against exposure was studied by monitoring the film resistance during exposure to atmosphere by continuously leaking air into the vacuum chamber using a needle valve. The leak rate was such that the pressure increased by an order of magnitude in about a minute.

Optical absorption spectra of the silver particulate films were obtained on a Shimadzu UV-Vis-NIR spectrophotometer model SHIMADZU UV 3101 PC.

Scanning electron microscopy (SEM) measurements were carried out on Scanning electron microscope model JEOL JSM 5800 CV with image processing software.

4. Results and discussion

4.1. Viscosity measurements

The effectiveness of dilute-solution viscometry is based on the assumption that mutual interactions of macromolecules in solution have a great influence on the viscosity in TPS (two polymers in a solvent) [11]. Therefore, compatibility among the polymers depends on the fact that the repulsive interactions among polymer molecules cause their shrinkage, leading to a lowering of solution viscosity, while attractive interaction increases the viscosity.

The relative and reduced viscosities of homopolymer and their blends are found out from viscometric measurements. The intrinsic viscosity values of homopolymers and their blends

were determined at 27^0 C in DMF by extrapolation to zero concentration of the plots of reduced viscosity (η_{sp}/C) versus concentration as shown in figure 1. The plots are not perfect linear, but no crossover is seen. A sharp crossover in the plots of reduced viscosity versus concentration indicates incompatibility of blends [27]. Therefore, some order of compatibility is expected in the blends.
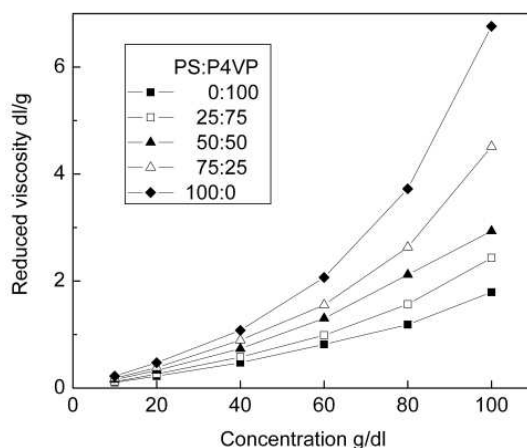

Figure 1. Reduced viscosity versus concentration composition of homopolymers in the blend for the PS/P4VP blends.

Figure 2. Relative viscosity versus original total concentration of 0.05g/ml.

Figure 2 shows a plot of relative viscosity versus blend composition at the original total concentration of 0.05g/ml. It is not found to be perfect linear for entire range. This indicates that the PS/P4VP blends are not hundred percent incompatible blend system [10, 28, 29].The concentration value is much lower than the critical concentration C″ estimated by C″ =1/ [η] [10].In the absence of specific interactions within the blend, polymer coils are independent if the solution concentration is below the critical concentration [10].The mixed solutions in DMF of PS and P4VP were clear indicating that no strong interactions are taking place between the blend components chains.

As proposed by Krigbaum and Wall [30], the specific viscosity η_{sp} of a solution polymer blends can be expressed as:

$$(\eta_{sp})_m = [\eta_1] C_1 + [\eta_2] C_2 + b_{11}C_1^2 + b_{22}C_2^2 + 2b_{12}C_1C_2 \tag{1}$$

Where $[\eta_1]$ and $[\eta_2]$ are the intrinsic viscosities of component polymers 1 and 2, C_1 and C_2 are the concentrations of polymers 1 and 2 in solution of polymer blend, b_{11} and b_{22} are specific interaction coefficients of polymers 1 and 2 in single polymer solutions and b_{12} is the interaction coefficient for the polymer blend of component polymers 1 and 2. The coefficient b_{11} is related to the constant k in the Huggins equation, when component polymer 1 is alone in the solution. This also applies to b_{22}.

$$\eta_{sp}/C = [\eta] + k[\eta]^2 C \tag{2}$$

The relationship between b_{11} and k can be written as

$$b_{11} = k_1 [\eta]^2 \tag{3}$$

Where k_1 is the Huggins constant for component polymer 1 in solution. The theoretical interaction coefficient between the two polymers, b_{12}^*, can be expressed as:

$$b_{12}^* = (b_{11} b_{22})^{1/2} \tag{4}$$

According to Krigbaum and Wall [30], information on the intermolecular interaction between polymer 1 and polymer 2 can be obtained by comparison of experimental b_{12} and theoretical b_{12}^* values. Hence, the miscibility of binary polymer blends can be characterized by the interaction parameter, Δb:

$$\Delta b = b_{12} - b_{12}^* \tag{5}$$

Negative values of Δb are found for solutions of incompatible polymer system, while positive values of Δb refer to attractive interaction in compatible systems. We can reduce the equation (1) to the following form when total concentration of the mixture (C) approaches zero.

$$(\eta_{spm}/C)_{c \to 0} = [\eta_1](C_1/C)_{c \to 0} + [\eta_2](C_2/C)_{c \to 0} \tag{6}$$

Polymer 1-polymer 2 interaction, Δb and theoretically $(\eta_{sp})_m$ can be calculated [15] as follows:

$$(\eta_{sp})_m / C_m = [\eta]_m + b_m C_m \tag{7}$$

Where C_m is the total concentration of polymers, C_1+C_2, and $[\eta]_m$ is the intrinsic viscosity of blend. It can be theoretically defined as;

$$[\eta]_m = [\eta]_1 X_1 + [\eta]_2 X_2 \tag{8}$$

Where X_1 and X_2 are weight fractions of polymer 1 and polymer 2, respectively. Interaction parameter, b_{12}, can be defined by the equation

$$b_m = X_1^2 b_{11} + X_1 X_2 b_{12} + 2 X_2^2 b_{22} \tag{9}$$

Where b_m defines the global interaction between all polymeric species. b_{12} may be obtained experimentally by Eq. (7).

All the calculated and experimental values are summed up in Table 1. The experimental intrinsic viscosity values are compared with their weighed average values and are found to be lower than the theoretical values. Shih and Beatty [29] have studied immiscible systems by this method and found that the intrinsic viscosity always shows a negative deviation due to the repulsive interaction between the polymers. Hence, these blends were not thermodynamically compatible under equilibrium conditions.

The repulsive deviation causes a reduction in the hydrodynamic volume of the polymer molecules, and hence, the viscosity of the solution is reduced. It is found that Δb values are very much less than unity and negative for all the blends except for the blend 25:75, for which slightly positive value of Δb predicting some order of compatibility. Also, positive deviation in 25:75 can be attributed to increase in the proportion of the polar group, P4VP in the blend [11]. The difference between η_1 and η_2 are found to be large and therefore, a more effective parameter μ can be defined to predict about the compatibility [28].

$$\mu = \Delta b / (\eta_2 - \eta_1)^2 \qquad (10)$$

Low values of μ observed in Table 1 may be due to weaker interaction between the polymers. The lower values of interaction parameters indicate that the PS and P4VP are not fully compatible, but physically miscible up to a certain extent.

Blend comp of PS/ P4VP	Intrinsic viscosity		Slope of red viscosity vs. concentration curve	Experimental Value, b_{12}	Theoretical value, b_{12}^*	Δb	μ
	Experimental(dl/g)	Theoretical(dl/g)					
0:100	0.167	0.167	0.018	-	-	-	-
25:75	0.284	0.402	0.024	0.053	0.034	0.019	0.021
50:50	0.325	0.638	0.03	0.017	0.034	-0.017	-0.019
75:25	0.64	0.874	0.045	0.018	0.034	-0.016	-0.017
100:0	1.11	1.11	0.067	-	-	-	-

Table 1. Intrinsic viscosity and interaction parametar of PS/P4VP blends.

4.2. Differential scanning calorimetery

DSC endothermograms for the homopolymers and their blends are shown in figure 3

All the blends exhibit a single T_g, intermediate between those of the parent polymers, PS and P4VP indicating the miscibility of these blends. The theoretical values of these can be predicted using Fox equation [31] and Gordon-Taylor equation [32].

$$1/T_g = X_1/T_{g1} + X_2/T_{g2} \qquad (11)$$

$$T_g = (X_1 T_{g1} + k X_2 T_{g2})/ (X_1 + k X_2) \qquad (12)$$
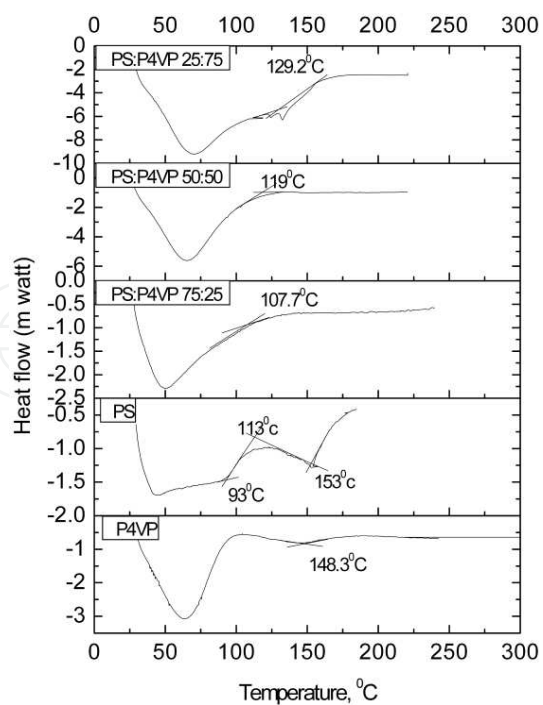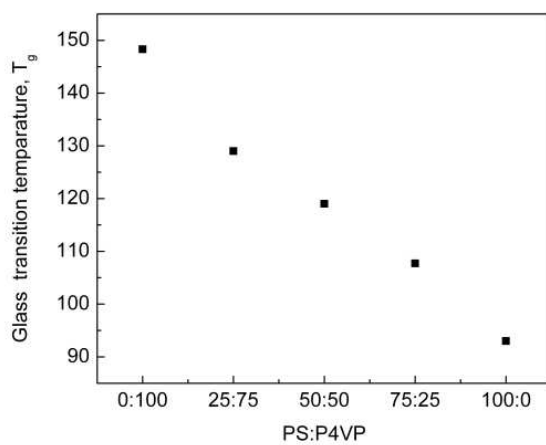
Figure 3. DSC thermograms of PS/P4VP blends

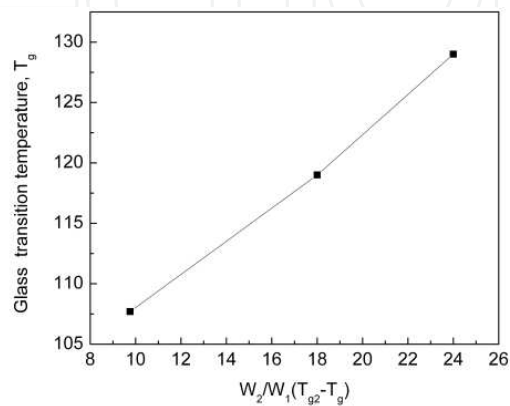**Figure 4.** Glass transition temperature versus composition of PS/P4VP.

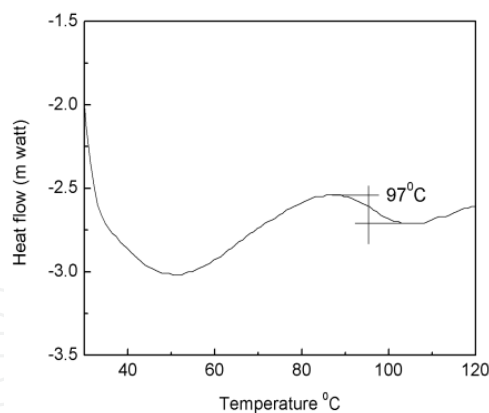**Figure 5.** Verification of Gordon- Taylor equation for PS/P4VP blends.

Figure 6. DSC thermogram of PS/P2VP, 50:50

Where X_1, X_2, T_{g1} and T_{g2} are the weight fractions and glass transition temperatures corresponding to polymer 1 and polymer 2, respectively. k is a constant which gives a semi-quantitative measure of degree of the interaction between the two polymers. All the experimental and calculated values of T_g, are shown in Table 2. Positive deviation observed from Fox equation is attributed to intermolecular interaction between the polymers. Figure 4 shows the plot of T_g, with blend composition. It is well established that when interactions between blend components are strong, such as those affected by Hydrogen bonding, the experimentally determined T_g of the blends are higher than those calculated from the additivity rule as a result of the reduction of polymer chains mobility in the blend [10]. In order to estimate the strength of the intermolecular interactions within the PS/P4VP blends, we used the Gorden-Taylor equation to verify through the linear fit in figure 5. Slope (k) of the straight line obtained is found to be 0.85, indicating interaction between the polymers [32]. The intercept is about 100.47^0 C which corresponds to T_g of pure PS.

Blend comp of PS/P4VP	Experimental T_g value (^{0}C)	Theoretical T_g value(^{0}C)
	DSC	Fox equation
0:100	148.3	-
25:75	129	125
50:50	119	116
75:25	107.7	107
100:0	93	-

Table 2. Experimental and theoretical glass transition temperatures of PS/P4VP blend.

Figure 6 shows DSC thermogram of the blend PS/P2VP, 50:50.This indicates a single T_g, about 370K intermediate between those of the parent polymers, PS and P2VP indicating the compatibility of the blend on melt mixing at higher temperature.

4.3. Fourier transform infrared spectroscopy

The proton donor PS copolymer, PSMAA (PS-methacrylic acid) with P4VP in solvent chloroform observed the specific interactions with the formation of hydrogen bonds, at a

frequency, υ = 1607 cm^{-1} corresponding to the –COOH…N≤ hydrogen bond [11]. Therefore, the incorporation of MAA into PS results in an augmentation in miscibility with P4VP, in comparison with the PS/P4VP system, which is highly incompatible [11]. The present solution cast PS/P4VP blends, needs to be applied in thin film form at higher temperature around 200^0 C. Therefore, we need to ascertain about their compatibility at higher temperature. Figure 7 is the FTIR of the sample of the polymer blend PS/P4VP, 50:50 before and after DSC being carried out. This shows the absorption bands at 1598 and 1414 cm^{-1} corresponding to the pyridine ring of P4VP and at 822 cm^{-1} to the single substituted pyridine appeared in the spectra of PS/P4VP blend. Similarly, for PS, the absorption peaks at 1493cm^{-1} and 1448 cm^{-1}, which were characteristic of the phenyl ring and the peak at 697cm^{-1}, corresponding to the signals of the single substituted phenyl ring, appeared for the blend as well. Similar trends were observed by the triblockpolymers PS-P4VP-PS and P4VP-PS-P4VP, which were synthesized by chain transfer agent [33]. In case of PS-block-P4VP, the stretching bands overlap [14].The silver particulate film deposited on PS/P4VP (50:50) resulted in desired structure underlying the property of PS and P4VP [34].Figure 7 shows no shift in the frequency leads to the absence of hydrogen bond. Thus, the possibility of protonation of nitrogen of P4VP [14] is ruled out but some intermolecular interaction at higher temperature leads to single Tg composition.

Figure 8 shows FTIR of PS/P2VP, 50:50 after DSC which clearly indicates the absorption bands at 1594 and 1414 cm^{-1} corresponding to the pyridine ring of PS and at 822 cm^{-1} to the single substituted pyridine ring appeared in the spectra of PS/P2VP blend. Similarly, the absorption peaks at 1495cm^{-1} and 1448 cm^{-1}, which were characteristic of the phenyl ring and the peak at 697cm^{-1}, corresponding to the signals of the single substituted phenyl ring for P2VP spectra, also appeared in the spectra of PS/P2VP, 50:50 blend. No shift in the frequency ruled out the possibility of any hydrogen bond in PS/P2VP. But single T$_g$ of the blend suggests some order of the compatibility at higher temperature.
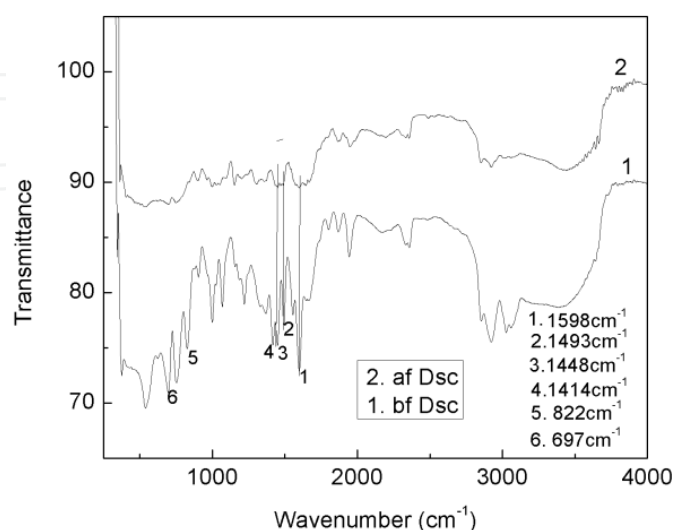

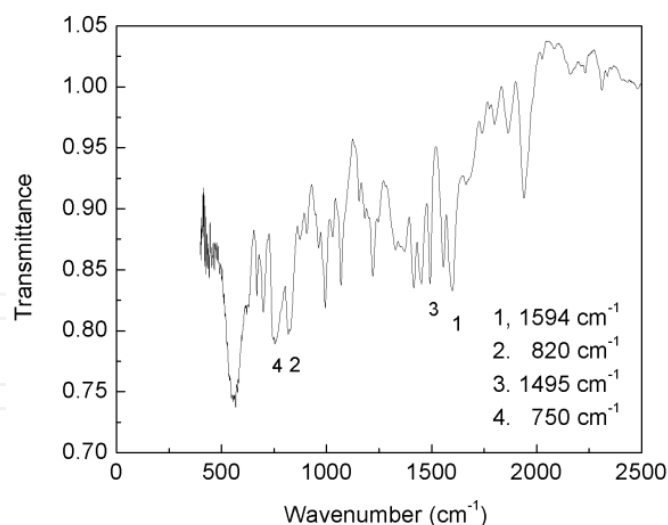**Figure 7.** FTIR for PS/P4VP (50:50) before and after DSC.

Figure 8. FTIR of PS/P2VP, 50:50 after DSC

4.4. Scanning electron microscopy

Fig. 9a and 9b show the SEM of PS: P4VP (50:50) samples after and before the DSC have been carried out. It is clear that after DSC the blend mixed better than the blend as obtained at room temperature by solution cast which eventually show phase separation after few days of preparation. Fig.9b clearly shows the dispersed phase of polymers whereas Fig. 9a indicates better compatibly of polymers. This can be attributed to mixing of homoplymers around 200⁰C during the process of DSC. This is an indication of suitable compatibility of these blends at higher temperature.

Figs. 10a and 10b are the Scanning Electron Micrographs of PS/P2VP, 50:50 samples before and after the DSC have been carried out. It is clear that melt mixing at higher temperature gives more compatible blend than room temperature solution mixed blend. Thus, an order of compatibility is achieved in PS/P2VP, 50:50 blend as reported for PS/P4VP blends [35]. Therefore, we can expect formation of discontinuous silver subsurface film on the blend.

4.5. Electrical behaviour of discontinuous silver films on PS/P2VP and PS/P4VP

Figure 11&12 shows the variation of the logarithm of resistance against inverse of temperature for silver films of different thicknesses deposited on polymers and their composite at a temperature of 457 K, during cooling to room temperature. It is interesting to note that while some of the films show only negative temperature coefficient of resistance (TCR) some show almost zero TCR. Some of the films show negative TCR at higher temperatures and almost zero TCR at lower temperatures. The 50 nm thick silver films on pure PS and 75:25 blend of PS/P4VP show negative TCR. Silver on PS showed similar behaviour in our earlier studies resulting in room temperature resistance same as that of the substrate with the formation of large silver particles separated by large distances [25]. Blending the inert polymer PS with an interacting polymer like P4VP to the extent of 25% does not seem to alter the morphology of the particulate film as indicated by the electrical
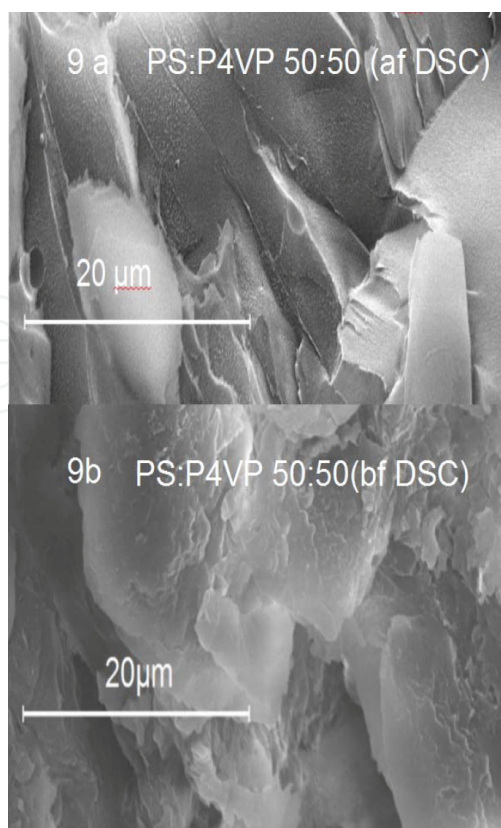
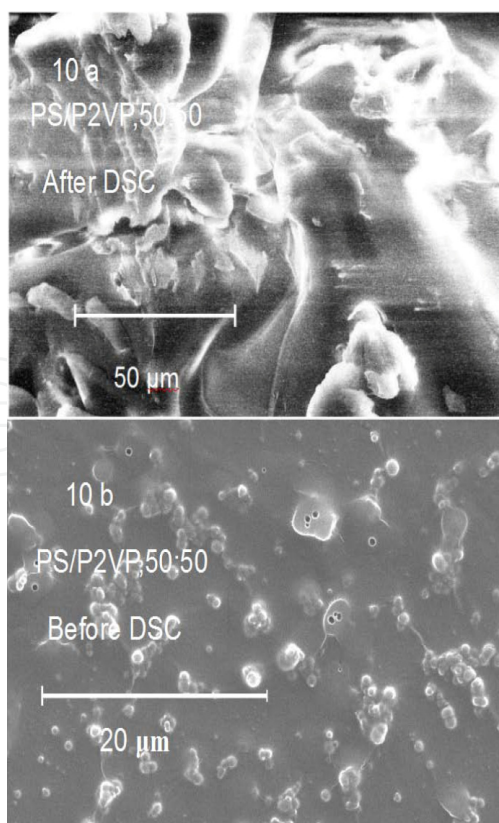**Figure 9.** SEM photographs of PS/P4VP (50:50) a. after DSC and b. before DSC.

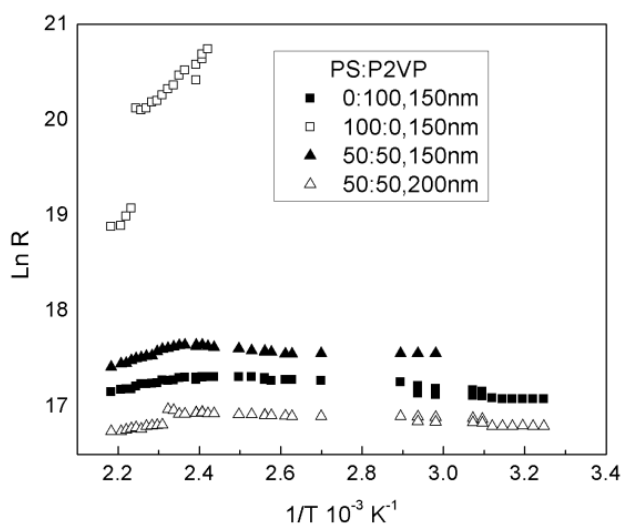**Figure 10.** SEM photographs of PS/P2VP, (50:50) (a) after and (b) before DSC.

Figure 11. Variation of ln R with 1/T for silver films deposited on the composite PS/P2VP held at 457 K at a rate of 0.4 nm/s.
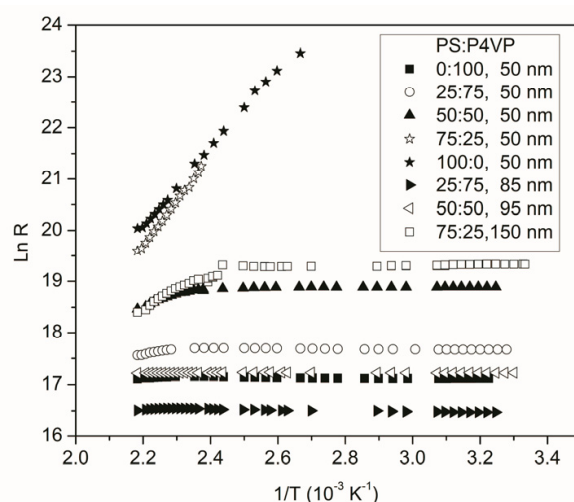

Figure 12. Variation of ln R with 1/T for silver films deposited on the composite PS/P4VP held at 457 K at a rate of 0.4 nm/s.

behaviour. When the P4VP content is increased to 50%, a negative TCR at high temperature followed by almost zero TCR at lower temperatures exhibited by the 50 nm thick film is similar to the behaviour observed earlier for the case of pure P2VP and P4VP [36, 37] indicating that the film consists of small particles separated by small distances. With further increase in P4VP content, the negative TCR part diminishes, giving rise to a near zero TCR .Similarly, the films on composites PS/P2VP (50:50) initially show negative TCR but zero TCR at lower temperature. Blending of PS with P2VP and P4VP seems to result in a positive effect on the composites. Therefore, negative TCR is totally vanishing and give rise to near zero TCR at room temperature for films deposited on the composites. The over all resistance of film deposited on composite decreases with increase in thickness of silver films deposited on the composite. Similar trend were reported that the electrical conductivity of composites is increased with high silver loading (30-80%) [38]. It is also interesting to note that even at 50% P4VP, with an increase of silver deposited, films show electrical characteristics as that

of the films on pure P4VP [37]. Further, when 150 nm thick silver is deposited on a polymer blend with only 25% of P4VP, the films show desirable electrical characteristics in contrast with the very high room temperature resistance observed for films on pure PS even at 300 nm of silver [25].

Figure 13&14 show the variation of logarithm of resistance (ln R) with logarithm of pressure in torr [ln (pressure)]. It is seen that the resistances show large increase beyond a pressure of about 0.5 torr, for all the films. The variation in resistance is very small till that pressure. Similar characteristics were shown by silver films on softened P4VP [39] and P2VP [36]. It was shown through X-ray photoelectron spectroscopy (XPS) studies at various electrons take off angles that silver clusters are formed at a depth of a couple of nm from the polymer surface [36,37]. It is known that the formation of subsurface particulate structure formation is subject to certain thermodynamic [6] and deposition conditions [5]. While the thermodynamic conditions are met for the deposition of metals on most of the polymer substrates, deposition conditions used in the present study are similar to those used in our earlier studies. Therefore, it is reasonable to assume that the particles are formed just a couple of nm below the polymer surface. The behaviour of the particulate films upon exposure to atmosphere is attributed to oxidation of islands due to the inadequate polymer cover.
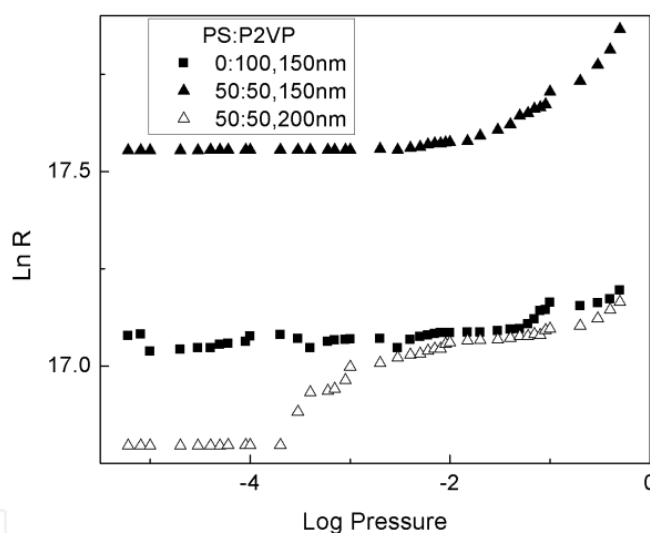

Figure 13. Variation of ln R with log (Pressure) for silver films deposited on composite PS/P2VP held at 457 K at a rate of 0.4 nm/s.

Figure 15 shows variation of room temperature resistance of silver particulate film of 150 nm thickness on PS/P2VP blends .It clearly indicates the decrease in resistance with increase in the amount of P2VP in the blend. Figure 16 shows variation of room temperature resistance of silver particulate film of various thicknesses on the blend PS/P2VP, 50:50.With the increase in the thickness of the silver particulate film the room temperature resistance of the film decreases [34]. Blending of P2VP with PS is expected to provide a polymer matrix where the size of silver clusters and inter-cluster separation can be modified because dispersion, size distribution and impregnation depth results from the natures of polymeric hosts [40].
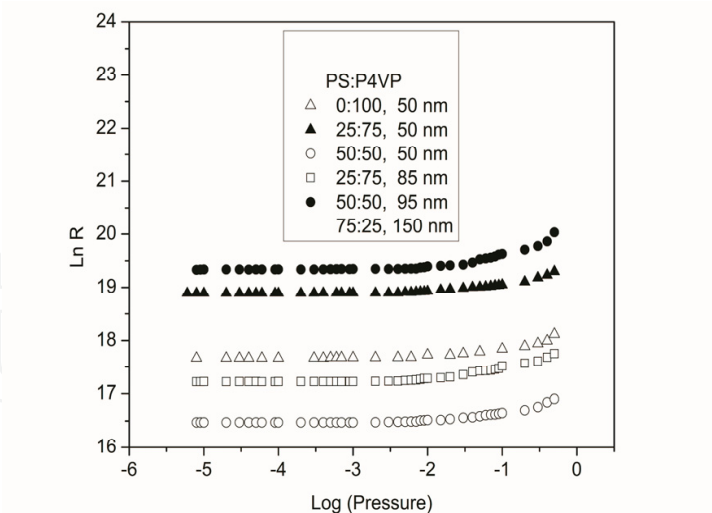
Figure 14. Variation of ln R with log (Pressure) for silver films deposited on composite PS/P4VP held at 457 K at a rate of 0.4 nm/s.
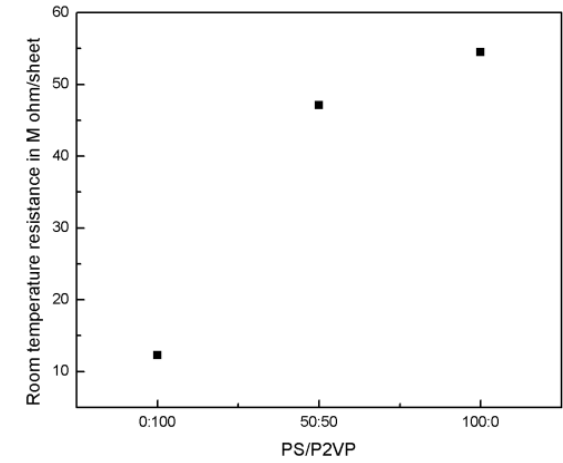

Figure 15. Variation of room temperature resistance of silver particulate film of 150 nm thickness verus composition of PS/P2VP.
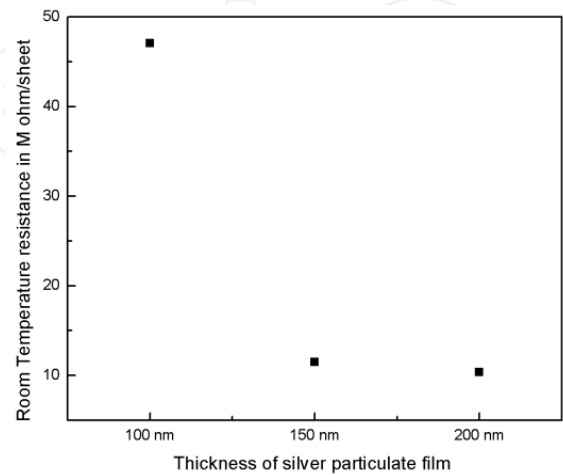

Figure 16. Variation of room temperature resistance of silver particulate film verus their thicknesses for PS/P2VP,50:50.

Figure 17 a,b,c shows the SEM of silver particulate films of thickness 200 nm on PS, P2VP and PS/P2VP, 50:50.It is evident from the figure that decrease in the particle size in the films of P2VP and PS/P2VP, 50/50 resulted in the close proximity of particles with reduction in the inter-particle separation. Also, the decrease in the size of silver cluster in the blend PS/P2VP, 50:50 improves the tunnelling effect as expected [34].Thus, the room temperature resistance of silver particulate film on the blend is now in the desirable range for applications.
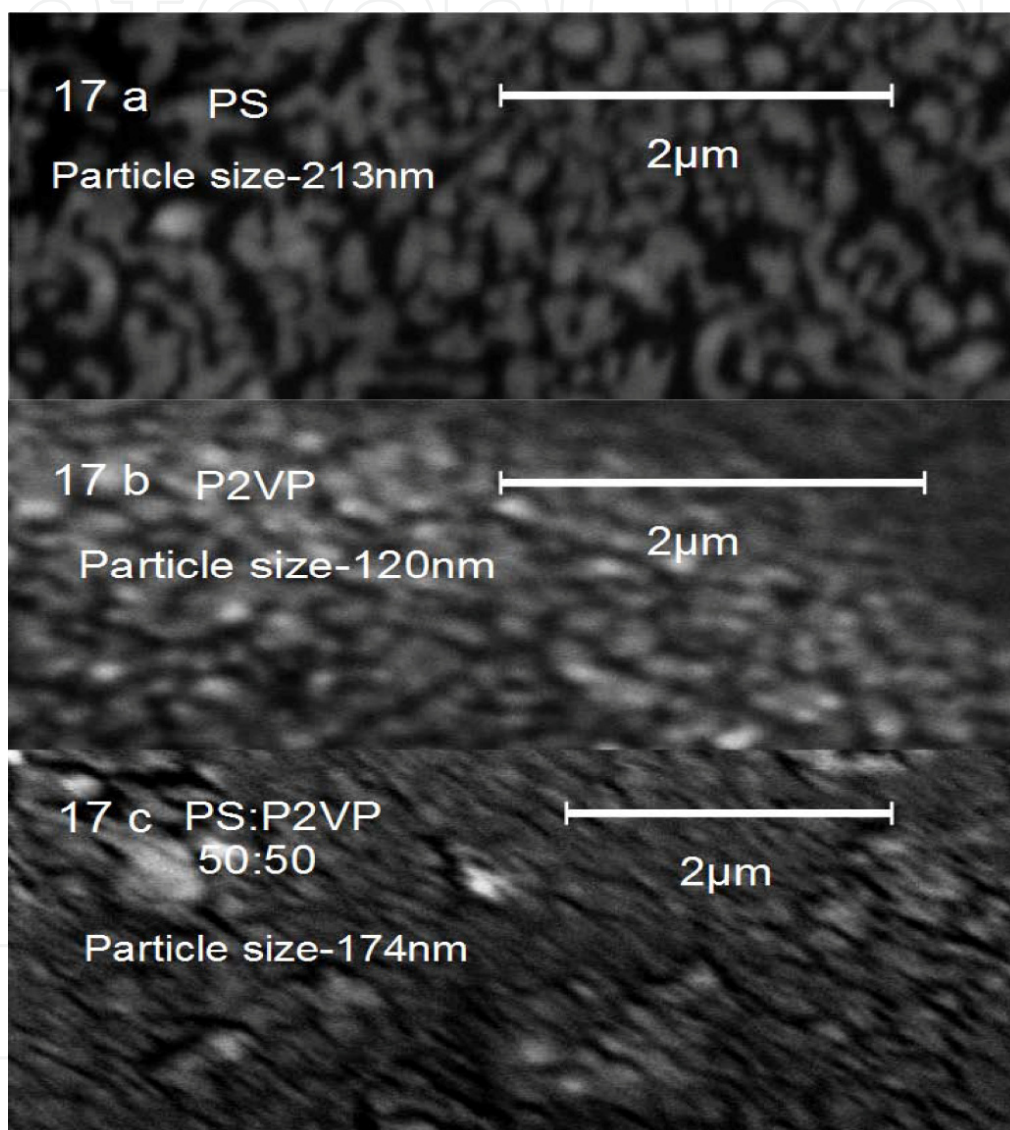

Figure 17. a,b,c: SEM of silver particulate films of thickness 200 nm on PS, P2VP and PS/P2VP, 50:50.

Figure 18 gives the variation of as deposited and room temperature resistances as a function of PS/P4VP composition for silver films of 50 nm thickness. It is seen that as the P4VP concentration increases there is a regular decrease of resistance at a fixed silver thickness. The plot of logarithm of these resistances with blend concentration gives linear fit as shown in figure19.Through this fit, one can estimate the resistance of the film at a particular blend and for the given conditions and thickness.
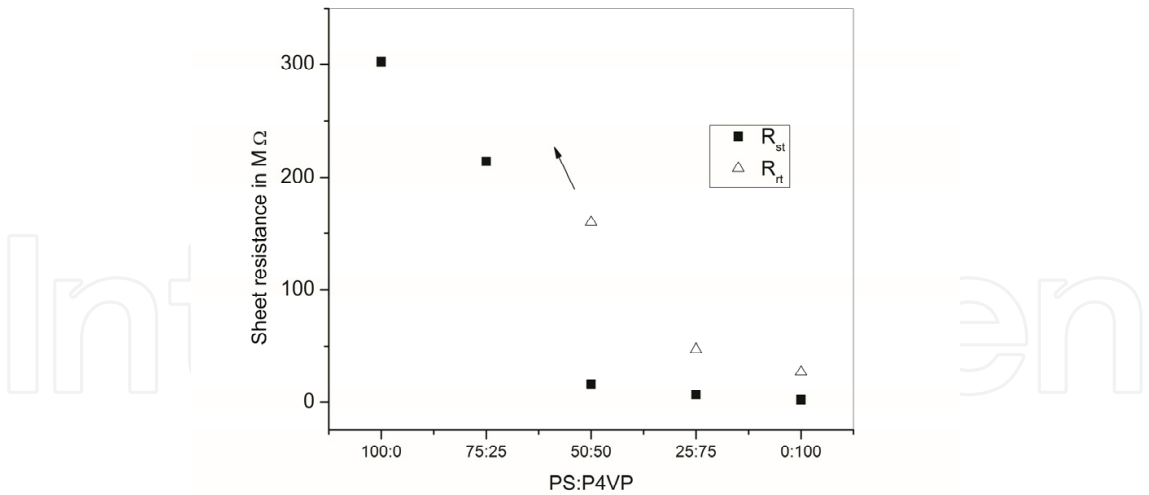
Figure 18. Variation of as-deposited and room temperature resistance with PS/P4VP blend composition for 50 nm silver films deposited at 457 K.
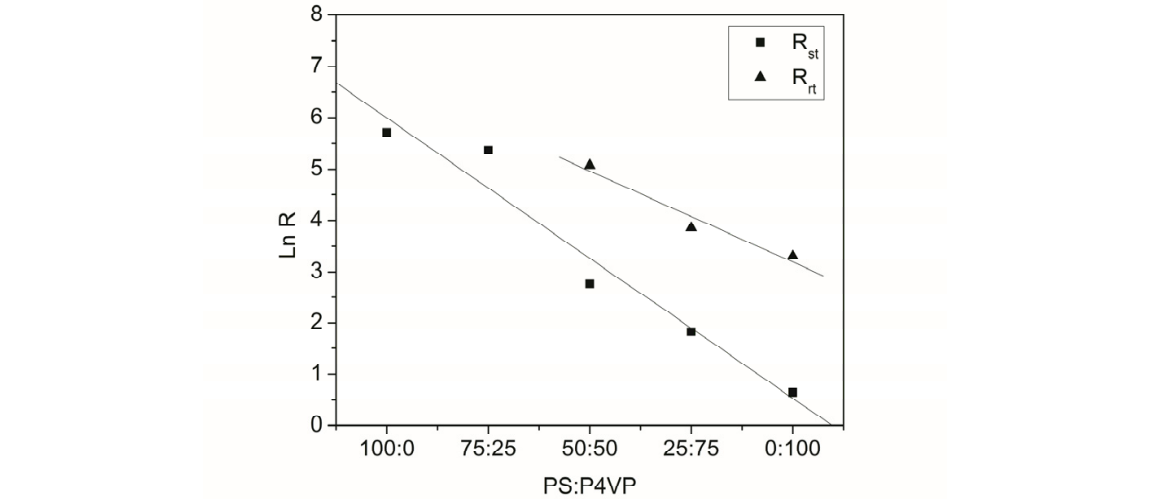

Figure 19. Variation of logarithm of resistances at 457 K and at room temperature with PS/P4VP blend composition for 50 nm silver films.

Table 3&4 gives the resistance data for the silver films of different thicknesses deposited on the PS/P2VP and P4VP, respectively.

Polymer PS:P2VP	Silver Film Thickness	Resistances	(MΩ/sheet)			
		R_{ts}	$R_{1\,hra}$	R_{rt}	$R_{0.5T}$	R_{atm}
0:100	100 nm	12.28	32.2	32.68	34.22	63.4
0:100	150 nm	9.73	28.08	26.13	30.53	45.64
50:50	100 nm	47.07	111.57	114.76	489	>1000
50:50	150 nm	11.5	34.98	42.04	57.4	76.56
50:50	200 nm	10.35	29.9	30.1	38.41	68.25
100:0	150 nm	54.46	159.3	-	-	-

Table 3. Resistances for silver films deposited on PS/P2VP blends held at 457 K with a rate of 0.4 nm/s.

Polymer PS:P4VP	Silver film thickness	Resistances (MΩ/□)				
		R_{st}	$R_{1\,hra}$	R_{rt}	$R_{0.5t}$	R_{atm}
0:100	50 nm	1.9	26.8	27.1	32.8	72.3
25:75	50 nm	6.2	42.2	47.1	73.7	1042
25:75	85 nm	3.2	14.7	14.2	21.9	215
50:50	50 nm	15.9	119.5	159.4	241.3	2465
50:50	95 nm	2.9	29.9	30.1	52.2	418
75:25	50 nm	214	325	-	-	-
75:25	150 nm	14.8	98.2	248.9	501.3	5172
100:0	50 nm	302	491	-	-	-

Table 4. Resistances for silver films deposited on PS/P4VP blends held at 457 K with a rate of 0.4 nm/s.

4.6. Morphology of silver particulate films on PS/P2VP and PS/P4VP blends

4.6.1. Optical studies

Fig. 20a shows the optical absorption spectra recorded for 100 nm silver films deposited on polymeric blends of PS/P2VP held at 457 K at the deposition rate of 0.4 nm/s. It is well known that small silver particles embedded in polymer matrix exhibit plasmon resonance absorption and as a result absorption maxima occur in the visible-near infrared region and their spectral position depends on the particle size, shape, filling factor etc. in the polymer matrix. The surface plasmon resonance absorption for silver clusters in the polymer matrix generally occurs at a wavelength of ~ 430 nm [8]. It is well known that shift in the plasmon resonance peak towards higher wavelength occurs due to close proximity of the silver clusters [41-44].These nanoparticles exhibit unique optical properties originating from the characteristic surface plasmon by the collective motion of conduction electrons [43,44].Thus, the formation of silver nanoparticles can also be confirmed by UV/VIS absorption spectrum of composite films [44].Spectral position, half width and intensity of the plasmon resonance strongly depend on the particle size, shape and the dielectric properties of the particle material and the surrounding medium [45].Thus, the type of metal and the surrounding dielectric medium play a significant role in the excitation of particle plasmon resonance (PPR). The sensitivity of PPR frequency to small variations of these parameters can be exploited in various applications [46]. The differing natures of the polymeric hosts yield change in dispersion, size distribution and impregnation depth of silver clusters [26]. Therefore, silver particles embedded in PS/P2VP blends, a shift of the resonance position to higher wavelength (red shift) were found, which were correlated with changes of particle sizes and inter-separation in silver clusters. It is clearly seen (Fig.20a) that the plasmon resonance peak shifts towards the longer wavelength side for the PS/P2VP, 50:50 (435) as compared to pure polystyrene (429 nm). Also, there is increase in intensity of absorbing peaks which signify the decrease of particles size with the incorporation of P2VP into PS [44].P2VP exhibits two peaks (441,606 nm). It is interesting to note that PS/P2VP, 50:50 also shows an additional absorption band at higher wavelength (616 nm). The possible explanation is that silver nanoparticles are in a highly aggregated state leading to coupling

of the plasmon vibrations between neighbouring particles [47].Similar results were found for silver particulate films of 150 and 200 nm films on PS/P2VP 50:50 blends. The shift in plasma resonance towards higher wavelength indicates close proximity and increase in particle size of silver nanoparticles with increasing thickness of silver particulate films [41].
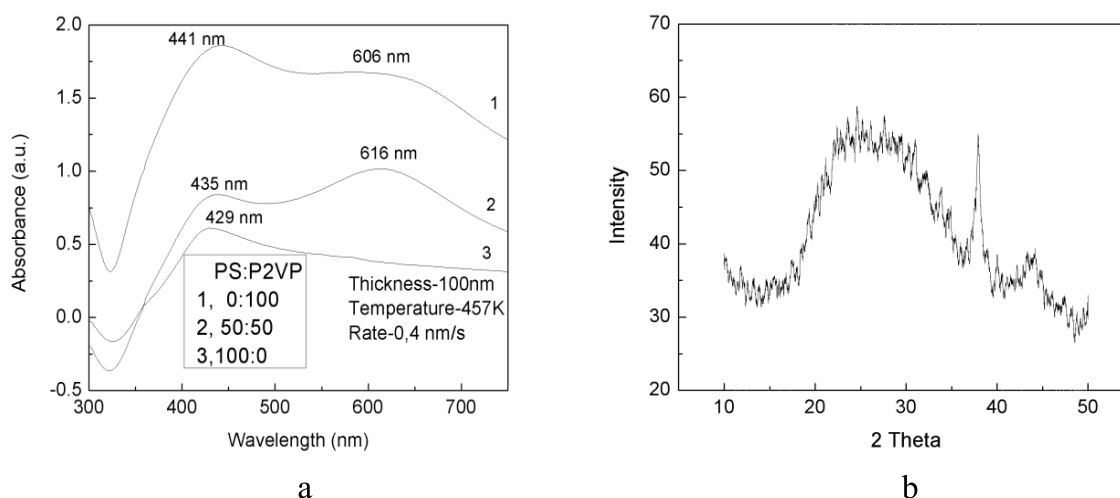

Figure 20. a: Optical absorption spectra for 100 nm silver particulate films deposited on PS/P2VP blends, **b**: XRD curve for silver particulate films of thickness 200 nm on PS/ P2VP, 50:50.

Fig.20 b shows the XRD pattern with the diffraction peak around 38^0 for the silver particulate films of thickness of 200 nm on PS/P2VP, 50:50. The broadening of the Bragg peaks indicates the formation nanoparticles. The particle sizes calculated from the Fig.20b is 40.6 nm for the silver particulate film of 200 nm on PS: P2VP, 50:50. The particle sizes estimated from XRD suggest that there is a small reduction in particle size due to blending of PS and P2VP. XRD of PS/P2VP, 50:50 for 200 nm has been carried out to have preliminary idea about average size of the silver clusters.

Fig. 21(a) shows the optical absorption spectra recorded for 50 nm silver films deposited on polymeric blends of PS/P4VP held at 457 K at the deposition rate of 0.4 nm/s. For silver particles embedded in PS/P4VP blends, a shift of the resonance position to higher wavelength (red shift) were found, which were correlated with changes of particle sizes and inter-separation in silver clusters. It is clearly seen (Fig.21a) that the plasmon resonance peak shifts towards the longer wavelength side in comparison to pure PS (485.5 nm).It is 598, 651.6 and 754.5 nm for PS: P4VP, 75:25, 50:50 and 25:75, respectively for 50 nm silver particulate films on them. Also, there is increase in intensity of absorbing peaks which can be attributed to the decrease of particles size with the incorporation of P4VP into PS [48].

Fig. 21 (b) shows the optical spectra recorded for the films of various thicknesses on PS/P4VP blends. The blend 50:50 shows the most promising result among all the silver particulate films on the blends. The intensity and shift of absorption peak is optimum (793 nm) for 95 nm film on PS/P4VP, 50:50.The silver particulate film of thickness 150 nm on PS/P4VP, 75:25 also shows a red shift (705 nm).This shift in the plasmon resonance peak towards higher wavelength can be attributed to close proximity of the silver clusters [42-45],

perhaps this is the reason for the better electrical behaviour of the film of thickness 150 nm on PS/P4VP, 75:25 [34].
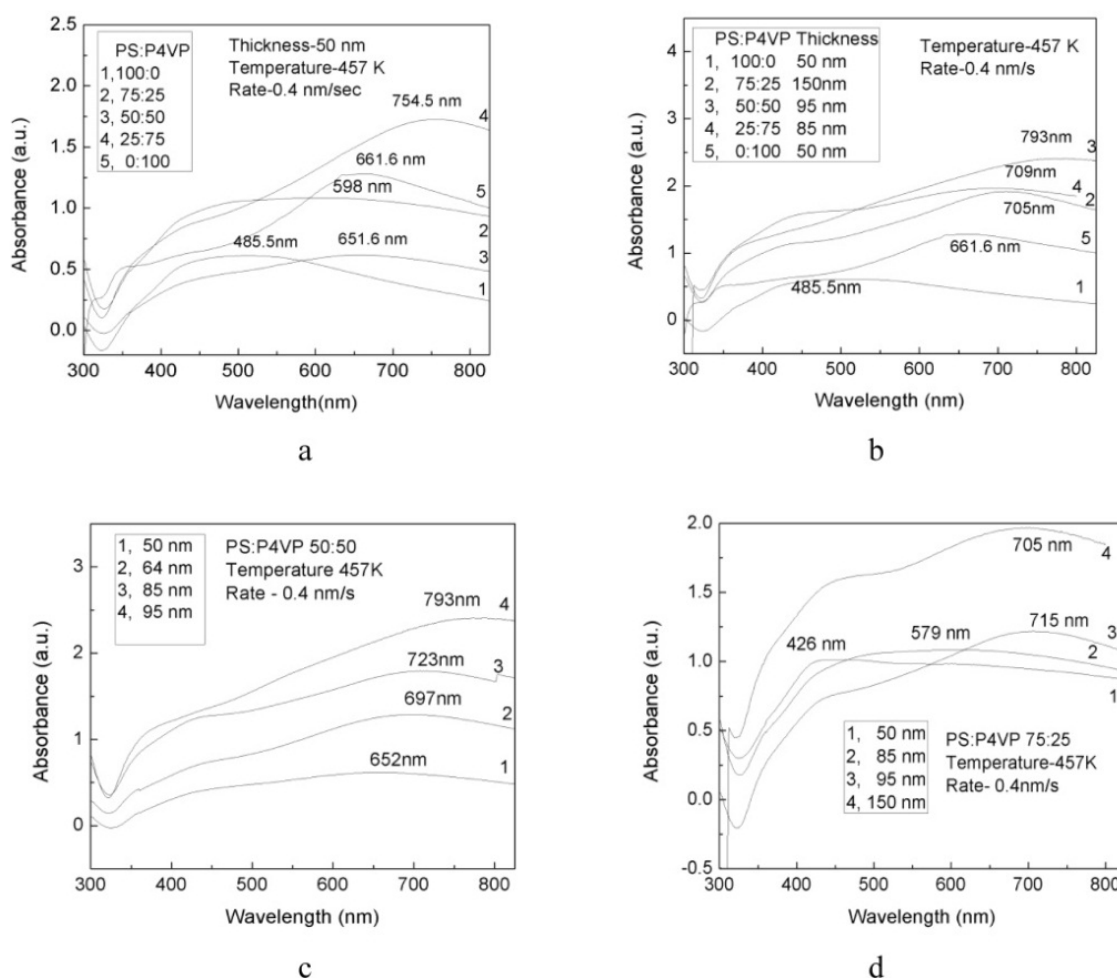

Figure 21. a Optical absorption spectra for 50 nm silver particulate films deposited on PS/P4VP blends, **b** Optical absorption spectra for the films of various thicknesses deposited on the PS /P4VP blends, **c** Optical absorption spectra for the films deposited on the blend PS/P4VP 50:50, **d** Optical absorption spectra for the film deposited on the blend PS/P4VP 75:25.

Fig. 21 (c) shows the optical spectra for films of varying thickness on PS/P4VP, 50:50.The shift in plasma resonance towards higher wavelength indicates close proximity of silver nanoparticles with increasing thickness of silver particulate films [15].

Fig. 21(d) shows the optical absorption spectra recorded for silver films on PS/P4VP, 75:25. It is clear that shift in surface plasma resonance is due to increase in particle size with the amount of silver deposited [8].The results are in agreement with the electrical properties of this blend which show increase in electrical conductivity on increasing silver loading [34].

As the fraction of the metal in a nanocomposite increases the nanoparticle separation decreases resulted in better electrical properties of nanocmposites [49]. Therefore, electrical behaviour of silver particulate films on PS/P4VP (50:50, 50 nm and 95 nm; 75:25, 50 nm and 150 nm) observed decrease in electrical resistance on increasing the thickness of film

[40].Thus, electrical studies of these blends suggest possibility of modification in morphology of silver particulate films on PS/P4VP as compared to films on PS.

Previous studies [8] of silver particulate films on PS for the 100 nm thickness exhibited minimum shift due to the presence of comparatively larger clusters with larger inter-cluster separations than on P2VP [8] for the same thickness. Also, silver particulate film on PS for the 50 nm thickness exhibited minimum shift due to the presence of comparatively larger clusters with larger inter-cluster separations than on P4VP [37] for the same thickness. Blending of P2VP with PS and P4VP with PS is expected to provide a polymer matrix where the size of silver clusters and inter-cluster separation can be modified because dispersion, size distribution and impregnation depth results from the natures of polymeric hosts [40].

Therefore, shift in the wavelength observed in optical spectra in the PS/P2VP, 50:50, and PS/P4VP, 75:25; 50:50; 25:75 can be attributed to modification in size distribution and better inter-cluster separations.
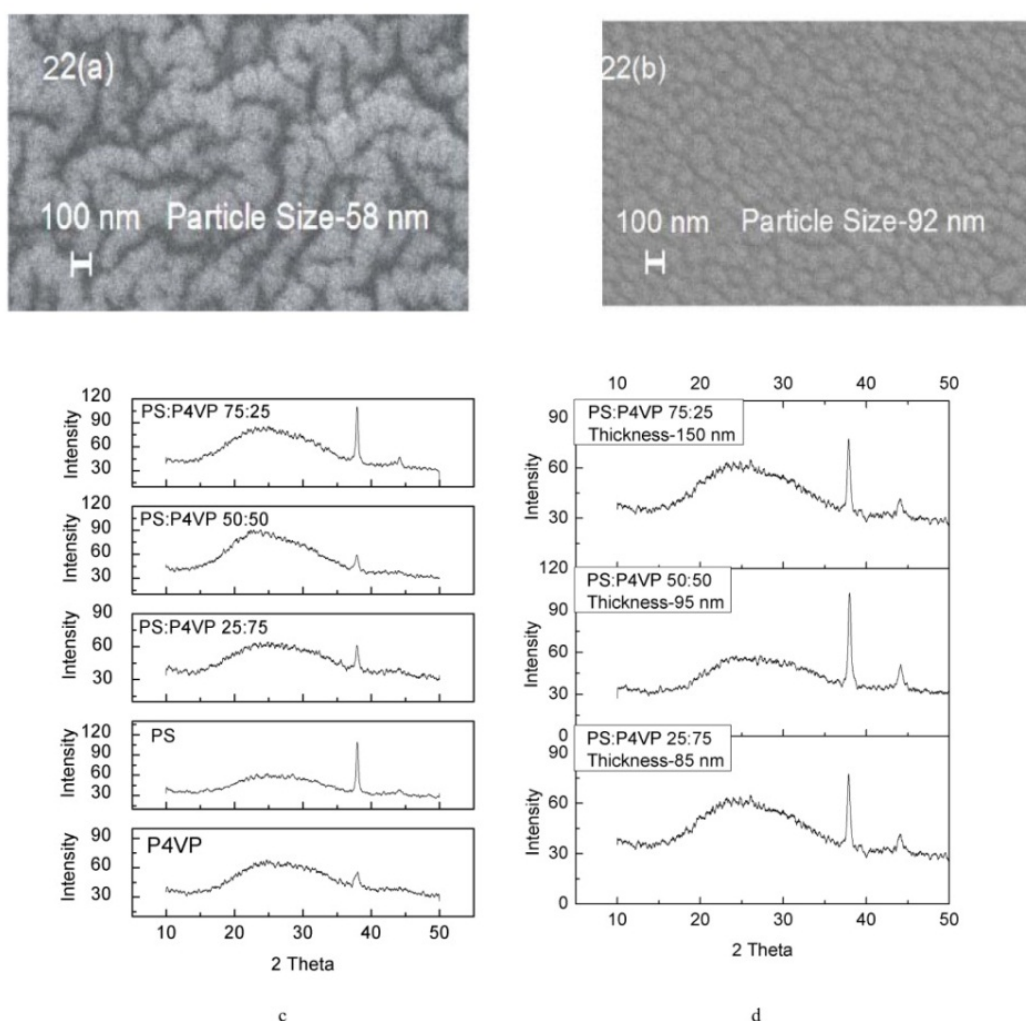

Figure 22. a,b: SEM images of PS/P4VP, (a) 0:100 and (b) 100:0 for silver particulate films of thickness 50 nm. Acceleration voltage- 20 kV, Magnification 50 KX, **c**: XRD curves for silver particulate films of thickness 50 nm on P4VP, PS, PS/ P4VP, 25:75, 50:50, 75:25, respectively. **d**: XRD curves for silver particulate films on PS/P4VP, 75:25, 50:50 and 25:75 for 150, 95 and 85 nm thicknesses, respectively

Fig.22c shows the XRD pattern with the diffraction peak around 38^0 for the silver particulate films of thickness of 50 nm on P4VP, PS and PS/P4VP, 25:75, 50:50, and 75:25. The broadening of the Bragg peaks indicates the formation nanoparticles. The particle sizes calculated from the Fig.22c are 53, 51, 49, 46 and 30 nm for the blends (PS: P4VP) 100:0, 75:25, 50:50, 25:75 and 0:100, in that order. The particle sizes estimated from XRD suggest that there is a very small reduction in particle size due to blending of PS and P4VP.Figure 22d shows the XRD patterns for the silver particulate films on PS/P4VP, 75:25, 50:50 and 25:75 for 150, 95 and 85 nm thicknesses, respectively. The reflections at 38^0 and 44^0 correspond to metallic silver. The particle sizes calculated from the Fig.22d are 52.3, 51.6 and 53 nm for the blends (PS: P4VP) 75:25, 50:50, and 25:75, respectively for the diffraction angle 38^0.

4.6.2. Micro structural studies

Electrical properties of polymer/metal composite films are strongly linked to particles' nanostructure [40]. As the fraction of the metal in a nanocomposite increases the nanoparticle separation decreases resulted in better electrical properties of nanocmposites [49-50,52,53]. SEM of the silver particulate films (Fig.22a & 22b) on homopolymers (PS, P4VP) clearly shows the characteristic nature of these polymers. The size and inter-separation of silver clusters is less (average particle size-58 nm) in P4VP whereas size as well as inter-separation is wide in PS (average particle size-92 nm). As a result, PS do not show the desired electrical conductivity [51].Blending of P2VP and P4VP into PS modifies size, size distribution and inter-separation of silver particles deposited on their blends PS/P2VP, 50:50 and PS/P4VP, 50:50 and 75:25. Therefore, electrical behaviour of silver particulate films on PS/P2VP, 50:50 for 100, 150 and 200 nm observed decrease in electrical resistance on increasing the thickness of films [52]. Thus, electrical studies of these blends suggest possibility of modification in morphology of silver particulate films on PS/P2VP and PS/P4VP as compared to films on PS.

SEM of the silver particulate films of 200 nm on the homopolymers (PS, P2VP) and their blend PS/P2VP, 50:50 were shown in the Fig.23a. The acceleration voltage is 30 kV and magnification is 60 to 100 KX for all the SEM pictures. The particle sizes measured from respective SEM pictures are plotted as histogram. The corresponding histograms (Fig.23a) of silver particles of the films are shown side by side of the SEM pictures. The data fit into a log normal distribution for all the cases. Hence, the average size, $\bar{a}$ and geometric standard deviation, σ_a are determined from the log normal distribution of the curves. The average size, $\bar{a}$ and geometric standard deviation, σ_a are 205 nm and 4; 109 nm and 9, 129 nm and 3, respectively, for silver films on PS, P2VP and their blend (50:50). The size distribution and width of histograms as shown in the figure indicate that the particle size varies from 100 to 400 nm, 60 to 180 nm and 60 to 200nm for silver films on PS, P2VP and their blend (50:50).It is clear from the figure that the size and inter-separation of silver clusters is wide in PS whereas size as well as inter-separation is less in P2VP [8]. As a result, PS do not show the desired electrical conductivity [36].Blending of P2VP with PS modifies size, size distribution and inter-separation of silver particles on their blend PS/P2VP, 50:50 which results in

improvement of tunnelling effect in the blend and the blend shows desired electrical behaviour [52]. This fact may be regarded as a consequence of the size as well as inter-separation evolution of nanoparticles during the ongoing deposition process.
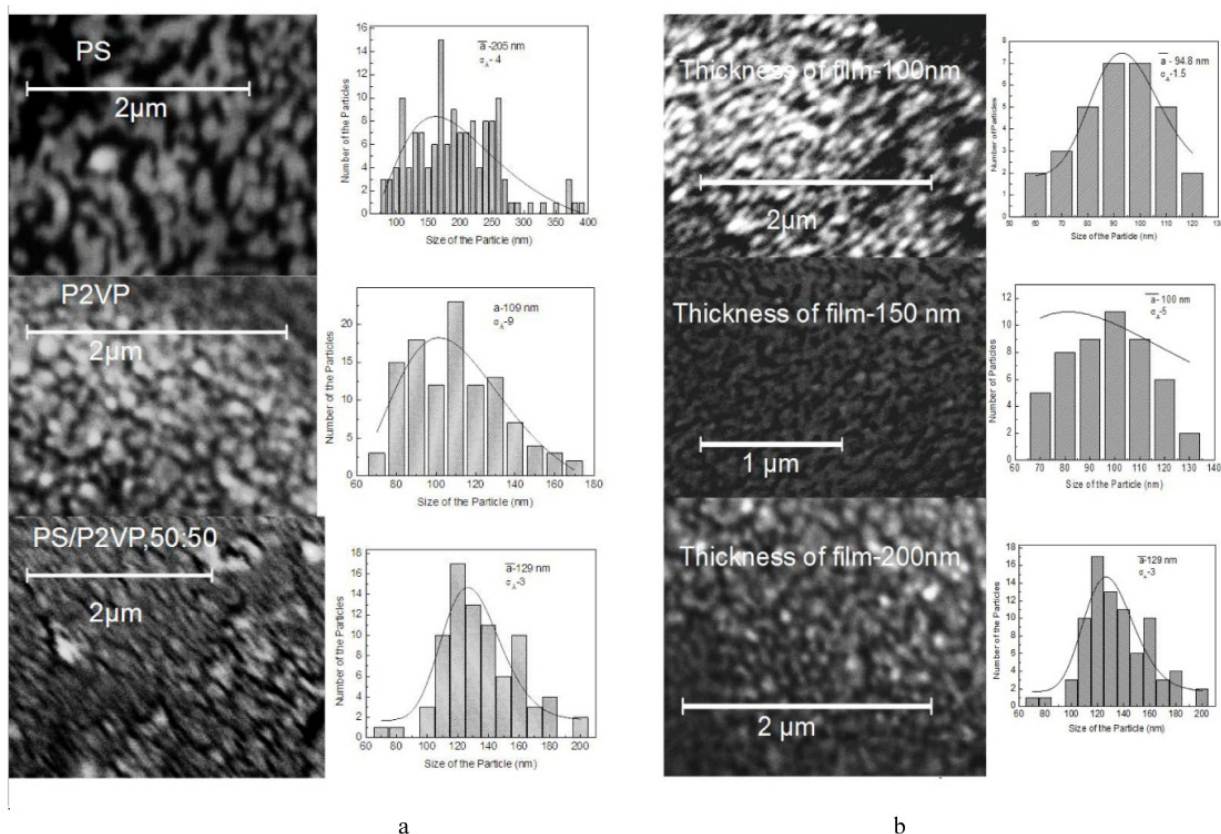

Figure 23. **a**: SEM of silver particulate films of 200 nm on PS, P2VP and PS/P2VP, 50:50 and their corresponding histograms. **b**: SEM of silver particulate films of 100, 150 and 200 nm on PS/P2VP, 50:50 and their corresponding histograms.

Fig.23b shows the particle size distribution for 100, 150 and 200 nm thickness films deposited on PS/P2VP, 50:50 and their corresponding histograms. The average size, $\bar{a}$ and geometric standard deviation σ_a are 94.8 nm, 1.5 and 100 nm, 5 and 129 nm, 3 for the 100, 150 and 200 nm film, respectively. It is evident from the figure that size distribution varied from 55-125, 65-135 to 70-200 nm for the 100, 150 and 200 nm films, respectively. Such dispersion of silver nanoparticle within the PS/P2VP, 50:50 leads to better electrical behaviour [52].This electric behaviour is not observed even for 300 nm silver particulate films on PS [20].Hence, silver particulate films on PS/P2VP, 50:50 at low volume fraction of silver consist of isolated and widely dispersed nanoparticles. But systematic and controlled increase of silver volume in the blend matrixes has shown increase in the size of silver clusters [52-53].

Figs.24a to 27a show the SEM pictures of various thicknesses of silver films deposited on PS/P4VP blends. The acceleration voltage is 20 kV and magnification is 50 to 100 KX for all the SEM pictures. The particle sizes measured from respective SEM pictures are plotted as histogram in figs. 24b to 27 b. The corresponding histograms (Figs.24b to 27 b) of silver particles of the films are shown side by side of the SEM pictures. The data fit into a log

normal distribution for all the cases. Hence, the average size, ā and geometric standard deviation, σ $_a$ are determined from the log normal distribution of the curves. The positive effect of blending P4VP with PS is clearly visible in these pictures. Figs. 24a, 25a show the particle size distribution for 50 and 95 nm thick silver films deposited on PS/P4VP, 50:50. The average size, ā and geometric standard deviation, σ $_a$ are 79.4 nm and ±1.2, respectively for the 50 nm film whereas the corresponding values for the 95 nm film are 95.4 nm and ±1.4. A closer look at the morphology of silver nanoparticles deposited on PS/P4VP, 50:50 in Figs.24a & 25a, clearly shows that particle size increases with the amount of silver deposited. The shape of the nanoparticles changes from near spherical particles to irregular ellipsoidal particles. The size distribution and width of histograms as shown in the figure indicate that the average size of the particle increases from 79.4 to 95.4 nm and the size distribution expands from 50-110 nm to 60-160 nm which results in improvement of tunnelling effect in PS/P4VP, 50:50 [40].And silver particulate film of thickness 95 nm show better electrical behaviour than silver particulate film of 50 nm on PS/P4VP, 50:50 [34]. It is evident that increase in size distribution decreases the inter-separation of silver clusters in this blend. This fact may be regarded as a consequence of the size as well as inter-separation evolution of nanoparticles during the ongoing deposition process.
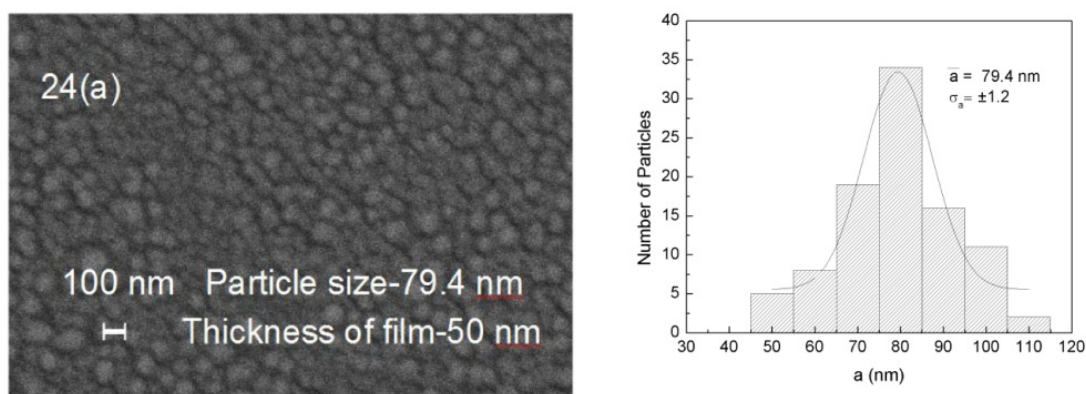

Figure 24. **a** SEM micrograph, Acceleration voltage-20 kV, Magnification 50 KX and **b** Corresponding histogram of 50 nm thick silver film on PS/P4VP, 50:50.
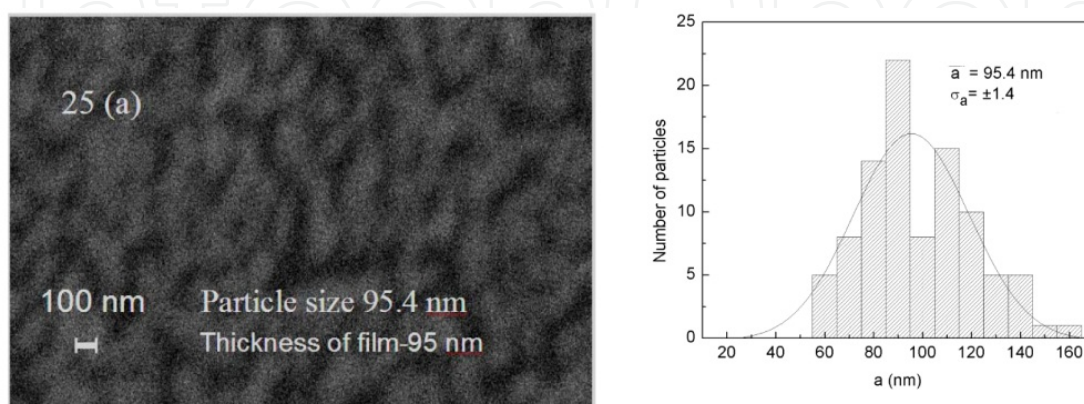

Figure 25. **a** SEM micrograph, Acceleration voltage-20 kV, Magnification 100 KX and **b** Corresponding histogram of 95 nm thick silver film on PS/P4VP, 50:50.

Figs.26a & 27a show the particle size distribution for 50 nm and 150 nm thickness films deposited on PS/P4VP, 75:25. The average size, ā and geometric standard deviation, σ $_a$ are 88.6 nm and ±8.5 for the 50 nm film and 96.7 nm and ±4 for 150 nm film, respectively. It is evident from the figure that distribution of size increased from 50-120 nm to 60-140 nm .Such dispersion of silver nanoparticle within the PS/P4VP, 75:25 leads to better electrical behaviour [40].Such electric behaviour is not observed even for 300 nm silver particulate film on PS [36].Hence, silver particulate film of 50 nm thickness on PS/P4VP, 75/25 consist of isolated and widely dispersed nanoparticles. But systematic and controlled increase of silver in the PS/P4VP, 75:25 matrixes produced interesting result [40]. The silver particulate film of thickness 150 nm on PS/P4VP, 75:25 shows the room temperature resistance in few mega ohms a desirable range for applications.

Figure 26. a SEM micrograph, Acceleration voltage-20 kV, Magnification 100 KX and **b** Corresponding histogram of 50 nm thick silver film on PS/P4VP, 75:25.

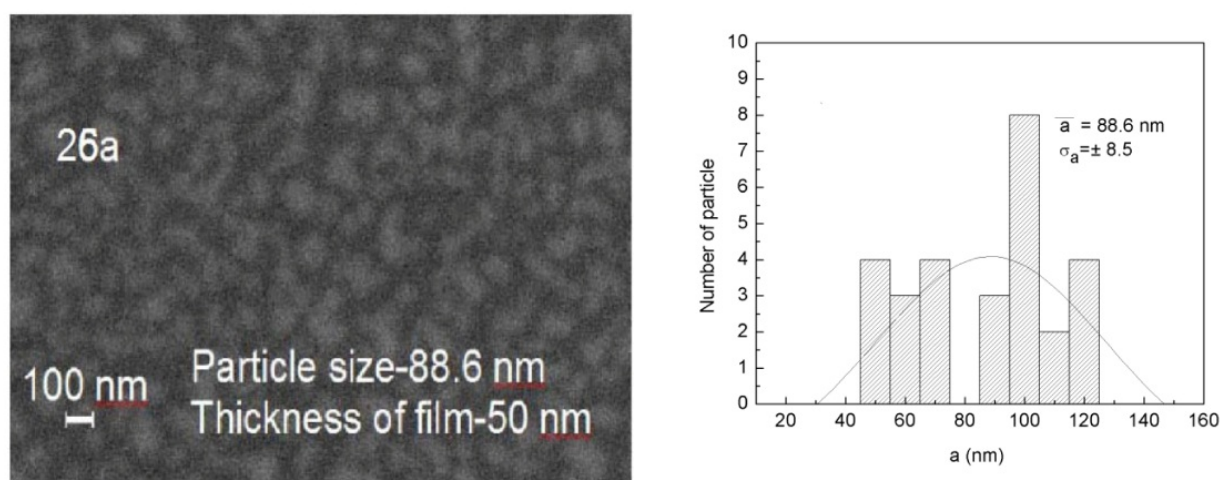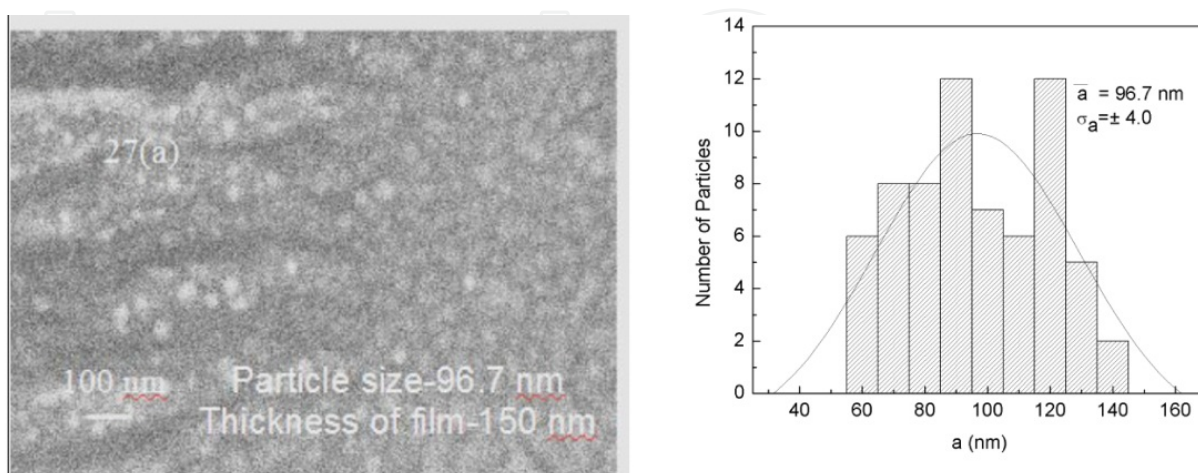**Figure 27. a** SEM micrograph, Acceleration voltage-20 kV, Magnification 100 KX and **b** Corresponding histogram of 150 nm thick silver film on PS/P4VP, 75:25.

Table 5&6 has been compiled to show all the particles size of silver clusters embedded in PS/P2VP and PS/P4VP blends from XRD and SEM. The SEM has provided the morphology of silver clusters and their distribution. The XRD diffraction pattern represents the average throughout the film due to increased penetration and large beam size. The observed values of particle size from SEM are in the same range as the calculated values of the particle size from XRD. The difference in the values may be due to averaging over longer depths because of penetration of X-rays. Though, the trend of particle size measured from XRD and SEM are similar.

PS/P2VP	Thickness (nm)	Particle size	(nm)	Standard deviation σ_a
		XRD	SEM, $\overline{a}$	
0:100	200		109	9
50:50	100	-	94.8	1.5
	150	-	100	5
	200	40.6	129	3
100:0	200		205	4

Table 5. The average particle size for silver deposited on PS/P2VP blends. The deposition rate is 0.4nm/s and temperature is 457K.

PS/P4VP	Thickness (nm)	Particle size	(nm)	Standard deviation σ_a
		XRD	SEM, $\overline{a}$	
0:100	50	30	58	-
25:75	50	46.6	-	-
	85	53	-	-
50:50	50	49.1	79.4	1.2
	95	51.6	95.4	1.4
75:25	50	51.8	88.6	8.5
	150	52.3	96.7	4.0
100:0	50	53.3	92	-

Table 6. The average particle size for silver deposited on PS/P4VP blends. The deposition rate is 0.4nm/s and temperature is 457K.

5. Further research

The silver films deposited on polymer composites show an increase in resistance, when they are exposed to atmosphere. It may be possible to stabilise the resistance against exposure to atmosphere through the deposition of good quality inorganic passivators like alumina, zirconia etc, to make the films suitable for device applications. Also, silver films are more

susceptible to oxygen in atmosphere than gold. Hence, deposition of gold nanopaticles on PS/P2VP and PS/P4VP composites may give more stabilised films which may be suitable films for sensitive applications.

6. Conclusion

The following conclusions may be drawn from the study on **Silver Particulate Films on Compatible Softened Polymer Composites**

Viscometry studies indicate a very small interaction parameter resulting in physically miscible blends of PS/ P4VP.DSC studies indicate a single T_g in all the cases indicating the formation of compatible blends. This may be due to some intermolecular interaction at higher temperature. Hence, the blends found some order of compatibility at higher temperatures. FTIR and SEM support the results of miscibility as well as DSC. The fairly compatible blend of PS/P2VP and PS/P4VP can be obtained on melt mixing at higher temperature. Deposition of silver on polymer blends coated substrate held at 457 K provides an approach to produce stable island films with reasonable control over their electrical resistance. Higher thickness films show almost zero TCR near room temperature, a desirable property for most of the devices. Low thickness films show a negative TCR, characteristic of island film. Silver particulate films deposited on composite blends show better electrical properties compared to pure PS.The deposition of silver particulate films by evaporation on PS/P2VP and PS/P4VP blends yields positive effect of blending PS with P2VP and P4VP.The size distribution and dispersion of silver nanoparticles is found to be dependent on the nature of the polymer host and thickness of particulate films. With the addition of P2VP, P4VP and amount of silver, morphology of the silver particulate films on PS/P2VP (50:50) and PS/P4VP (50:50, 75:25) could be modified to give the desired electrical results.

Author details

Pratima Parashar
Department of Materials Science, Mangalore University, Mangalagangotri, India
CET, IILM Academy of Higher Learning, Greater Noida, India

Acknowledgement

7. References

[1] Skofronick J G, Phillips W B (1967) Morphological Changes in Discontinuous Gold Films following Deposition. J. Appl. Phys. 38(12): 4791-4796.

[2] Fehlner F P (1967) Behavior of Ultrathin Zirconium Films upon Exposure to Oxygen. J. Appl. Phys. 38: 2223- 31.

[3] Kovacs G J, Vincent P S (1982) Formation and Thermodynamic Stability of a Novel Class of Useful Materials: Close-Packed Monolayers of Submicron Monodisperse Spheres Just below a Polymer Surface. J. Colloid. Interface. *Sci*. 90: 335-342.

[4] Kovacs G J, Vincentt P S (1983) Subsurface particulate film formation in softenable substrates present status and possible new applications. Thin Solid Films 100: 341-353.

[5] Kovacs G J, Vincentt P S, Trumblay C, Pundsak A L (1983) Vacuum deposition onto softenable substrates formation of novel subsurface structures.Thin Solid Films 101: 21-40.

[6] Kovacs G J, Vincentt P S (1984) Subsurface particulate film formation in softenable substrates present status and possible new applications.Thin Solid Films 111: 65-81.

[7] Kunz M S, Shull K R Kellock A J (1992) Morphologies of Discontinuous Gold Films on Amorphous Polymer Substrates. J. Appl. Phys. 72: 4458-4460.

[8] Mohan R K, Pattabi M (2001) Effect of polymer-metal particle interaction on the structure of particulate silver films formed on softened polymer substrates. J. New Mat. Electrochem. Systems 4: 11-15.

[9] Yuan JJ, Ma R, Gao Q, Wang YF, Cheng SY, Feng LX, Fan Z Q, Jiang L (2003) Synthesis and characterisation of Polystyrene/ Poly(4-vinylpyridine) Triblock Copolymers by Reversible Addition –Fragmentation Chain Transfer Polymerisation and Their Self-Assembled Aggregates in Water. J Appl Polymer Sci, 89:1017-1025.

[10] Bouslah N, Amrani F (2007) Miscibility and specific interactions in blends of poly [(styrene)-co-(cinnamic acid)] with poly (methyl methacrylate) and modified Poly(methyl methacrylate).Express polymer letters 1:44-50.

[11] Torrens F, Soria V, Codoner A, Abad C, Campos A (2006) Compatibility between polystyrene copolymers and polymers in solution via hydrogen bonding. Euro polymer Journal 42(10): 2807-2823.

[12] Bouslah N, Hammachin R, Amrani F (1999) Study of the compatibility of poly[styrene-*co*-(cinnamic acid)]/poly[(ethyl methacrylate)-*co*-(2-dimethylaminoethyl methacrylate)] blends. Macromolecular Chemistry and Physics 200(4):678-682.

[13] Jiao H, Goh S H, Valiyaveettil S (2001) Mesomorphic Interpolymer complexes and blends based on poly (4-vinylpyridine)- dodecylbenzenesulfonic acid complex and poly(acrylic acid) or poly(p-vinvylphenol. Macromolecules, 34:7162-7165.

[14] Kosonen H, Valkama S, Hartikainen J, Eerikainen H, Torkkel M, Jokela K, Serimaa R, Sundholm F, Brinke G, Ikkala O (2002) Mesomorphic Structure of Poly(styrene)-block-poly(4-vinylpyridine) with Oligo(ethylene oxide)sulfonic Acid Side Chains as a Model for Molecularly Reinforced Polymer Electrolyte. Macromolecules 35: 10149-10154.

[15] Wang X, Zuo J, Keil P, Grundmeier G (2007) Comparing the growth of PVD silver nanoparticles on ultra thin fluorocarbon plasma polymer films and self-assenbled fluoroalkyl silane monolayers. Nanotecnology 18:265303-265313.

[16] Heilmann A (2002) Polymer Films with Embedded Metal Nanoparticles, Berlin:Springler.

[17] Mayer A B R (2001) Colloidal metal nanoparticles dispersed in amphiphilic polymers. Polym. Adv. Technol. 12: 96-106.

[18] Beecroft L L (1997) Nanocomposite materials for optical applications. Chem.Mater. 9:1302-1317.

[19] Caseri W (2000) Nanocomposites of polymers and metals or semiconductors: Historical background and optical Properties Macromol.Rapid Commun. 21:705-722.

[20] Eilers H, Biswas A, Pounds T D, Norton M G (2006) Teflon AF/Ag nanocomposites with tailored optical properties. J.Mater. Res 21:2168-2171.

[21] Yonzon C R, Stuart D A, Zhang X, Mcfarland A D, Haynes CL, Duyne R P V (2005) Towards advanced chemical and biological nanosensors—An overview. Talanta 67:438-448.

[22] Saito R, Okamura S, Ishizu K (1992) Introduction of colloidal silver into a poly (2-vinyl pyridine) microdomain of microphase separated poly(styrene-*b*-2-vinyl pyridine) film. Polymer 33(5):1099-1101.

[23] Tao L, Ho R M, Ho J C (2009) Phase Behavior in Self-assembly of Inorganic/Poly(4-vinylpyridine)-b- Poly (ε-caprolactone) HybridMacromolecules 42:742-751.

[24] Pennelli G (2006) Lateral reduction of random percolative networks formed by nanocrystals: Possibilities for a new concept electronic device. Appl. Phys. Lett. 89:163513-163516.

[25] Rao K M, Pattabi M, Mayya K S, Sainkar S R, Murali Sastry M S (1997) Preparation and characterization of silver particulate films on softened polystyrene substrates. Thin Solid Films 310: 97

[26] Hassell T, Yoda S, Howdle S M., Brown P D (2006) Microstructural charecterisation of silver/polymer nanocomposites prepared using supercritical cabondioxide. J. of Phys: Conference Series 26:276-279.

[27] Dondos A S, Kondras P, Pierri P, Benoit H (1983) Hydrodynamic crossover in two-polymer mixtures from viscosity measurement. Macromolek Chem, 184(10):2153-2158

[28] Rao V, Ashokan P, Shridhar M H (1999) Studies on the compatibility and specific interaction in cellulose acetate hydrogen phthalate (CAP) and poly methyl methacrylate (PMMA) blend. Polymer 40:7167-7171.

[29] Shih K S, Beatty C L (1990) Blends of polycarbonate and poly(hexamethylene sebacate): IV. Polymer blend intrinsic viscosity behavior and its relationship to solid-state blend compatibility. Br Polym. J. 22 (1):11-17.

[30] Krigbaum W R, Wall F T (1950) Viscosities of binary polymeric mixtures. J Polym Sci. 5:505-514.

[31] Fox, T G (1956) Influence of Diluent and of Copolymer Composition on the Glass Temperature of a Polymer System..Bull Am Phys Soc. 1:123-125.

[32] Gordon M, Taylor J S (1952) Ideal copolymers and the second-order transitions of synthetic rubbers. I. Non-crystalline Copolymers. J Appl Chem 2:493-500

[33] Dong H.K, Won H.J, Sang C L, Ho C.K (1998) The compatibilizing effect of poly(styrene-*co*-4-vinylpyridine) copolymers on the polystyrene–polyethylene-based ionomer blends. J Appl. Polymer Sci. 69:807- 816.

[34] Parashar P, Pattabi M, Gurumurthy S C (2009) Electrical behaviour of discontinuous silver films deposited on softened polystyrene and poly (4-vinylpyridine) blends. J.Mater.Sci:Mater Electron 20: 1182-1185.

[35] Parashar P, Ramakrishna K, Ramaprasad A T (2011) A Study on Compatibility of Polymer Blends of Polystyrene/Poly(4-vinylpyridine). Journal of Appl Poly Sci 120 (3):1729-1735.

[36] Pattabi M, Rao K M, Sainker S R, Sastry M (1999) Structural studies on silver cluster films deposited on softened PVP substrate. Thin Solid Films 338:40-45.

[37] Rao K M, Pattabi M., Sainkar S. R, Lobo A., Kulkarni S K, Uchil J, Sastry M. S (1999) Preparation and characterisation of silver particulate structure deposited on softened poly(4-vinylpyridine) substrate. J. Phys. D: Appl.Phys. 32:2327-2336.

[38] Haoyan W, Eilers H (2008) Electrical Conductivity of Thin-Film Composites Containing Silver nanoparticles Embedded in a Dielectric Teflon AF Matrix. Thin Solid Films, 517: 575-581.

[39] Pattabi M , Rao K M (1998) Electrical behaviour of discontinuous silver films deposited on softened polyvinyl pyridine Substrate. J. Phys. D: Appl. Phys. 31: 19-23.

[40] Kiesow A, Morris J E, Radehaus C, Heilmann A (2003) Switching behavior of plasma polymer films containing silver nanoparticles. J.Appl. Phy. 94 (10): 6988-6990.

[41] Heilmann A, Kiesov A,Gruner M, Kreibig U (1999) Optical and electrical properties of embedded silver nanoparticles at low temperatures.Thin Solid Films 343-344:175-178.

[42] Fritzsche W, Porwol H, Wiegand A, Boronmann, Khler J M (1998) In-situ formation of Ag-containing nanoparticles in thin polymer film. Nanostrutured Materials, 10 (1) 89-97.

[43] Akamatsu K, Takei S, Mizuhata M, Kajinami A, Deki S, Fujii M, Hayashi S, Yamamoto K (2000) Preparation and characterization of polymer thin films containing silver and silver sulfide nanoparticles.Thin Solid Films 359:55-60.

[44] Carotenuto G (2001) Synthesis and characterization of poly (*N*-vinylpyrrolidone) filled by monodispersed silver clusters with controlled size. Appl. Organometal. Chem. 15(5):344-351.

[45] Kim J Y, Shin D H, Ihn K J, Suh K D (2003) Amphiphilic Polyurethane-co-polystyrene Network Films Containing Silver Nanoparticles. J Ind. Eng. Chem. 9(1):37-44.

[46] Heilmann A, Quinten M, Werner J (1998) Optical response of thin plasma-polymer films with non-spherical silver nanoparticles Eur.Phys. J.B, 3:455-461.

[47] Mandal S, Arumgam S K, Pasricha R, Sastry M (2005) Silver nanoparticles of variable morphology synthesized in aqueous foams as novel templates. Bull. Mater. Sci. 28(5):503-510.

[48] Kim JY, Shin DH, Ihn KJ (2005) Synthesis of CdS nanoparticles dispersed within amphiphilic poly(urethane acrylate-*co*-styrene) films. J.Appl.Polym Sci. 97(6):2357-2363.

[49] Biswas A, Bayer I S, Marken B, Pounds D, Norton M G (2007) Networks of ultra-fine Ag nanocrystals in a Teflon AF® matrix by vapour phase e-beam-assisted deposition Nanotecnology 18:305602-305608.

[50] Parashar P (2011) Morphology of Silver Particulate Films Deposited on Softened Polymer Blends of Polystyrene and Poly (4-vinylpyridine)J.Appl.Polymer Sci. 121 (2): 839-845.

[51] Takele H, Greve H, Pochstein, Zaporojtchenko V, Faupel F (2006) Plasmonic properties of Ag nanoclusters in various polymer matrices. Nanotechnology 17: 3499-3505.

[52] Parashar P (2011) Electrical behaviour of discontinuous silver films deposited on compatible Polystyrene/Poly (2- vinylpyridine) composite. J.Mater.Sci:Mater Electron, DOI 10.1007/s10854-011-0418-6.

[53] Parashar P (2011) Structural properties of silver particulate films deposited on softened polymer blends of polystyrene/poly (2-vinyl pyridine) J.Mater.Sci:Mater Electron, DOI 10.1007/s10854-011-0567-7